Reproducible 3D culture of multicellular tumor spheroids in supramolecular hydrogel from cancer stem cells sorted by sedimentation field-flow fractionation

Tarek Saydé, Omar El Hamoui, Bruno Alies, Gaëlle Bégaud, Barbara Bessette, Sabrina Lacomme, Philippe Barthélémy, Gaëtane Lespes, Serge Battu, Karen Gaudin

Journal of Chromatography A 1736 (2024) 465393

Contents lists available at ScienceDirect

Journal of Chromatography A

journal homepage: www.elsevier.com/locate/chroma

Reproducible 3D culture of multicellular tumor spheroids in supramolecular hydrogel from cancer stem cells sorted by sedimentation field-flow fractionation

Tarek Saydé [a,b,1], Omar El Hamoui [b,c,1], Bruno Alies [b,*], Gaëlle Bégaud [a], Barbara Bessette [a], Sabrina Lacomme [d], Philippe Barthélémy [b], Gaëtane Lespes [c], Serge Battu [a,*], Karen Gaudin [b]

[a] Université de Limoges, UMR INSERM 1308 CAPTuR, Faculté de Médecine, 87025 Limoges, France
[b] Université de Bordeaux, INSERM U1212, UMR CNRS 5320, F-33076 Bordeaux, France
[c] Université de Pau et des Pays de l'Adour (E2S/UPPA) CNRS, IPREM, UMR 5254, 64053 Pau Cedex, France
[d] Bordeaux Imaging Center, UMS 3420 CNRS-INSERM, Université de Bordeaux, Bordeaux 33076, France

ARTICLE INFO

Keywords:
Cancer stem cells
Multicellular tumor spheroids
Sedimentation field-flow fractionation
Cell sorting
Supramolecular hydrogel

ABSTRACT

Three-dimensional (3D) cancer models, such as multicellular tumor spheroids (MCTS), are biological supports used for research in oncology, drug development and nanotoxicity assays. However, due to various analytical and biological challenges, the main recurring problem faced when developing this type of 3D model is the lack of reproducibility. When using a 3D support to assess the effect of biologics, small molecules or nanoparticles, it is essential that the support remains constant over time and multiples productions. This constancy ensures that any effect observed following molecule exposure can be attributed to the molecule itself and not to the heterogeneous properties of the 3D support. In this study, we address these analytical challenges by evaluating for the first time the 3D culture of a sub-population of cancer stem cells (CSCs) from a glioblastoma cancer cell line (U87-MG), produced by a SdFFF (sedimentation field-flow fractionation) cell sorting, in a supramolecular hydrogel composed of single, well-defined molecule (bis-amide bola amphiphile 0.25% w/v) with a stiffness of 0.4 kPa. CSCs were chosen for their ability of self-renewal and multipotency that allow them to generate fully-grown tumors from a small number of cells.

The results demonstrate that CSCs cultured in the hydrogel formed spheroids with a mean diameter of 336.67 ± 38.70 μm by Day 35, indicating reproducible growth kinetics. This uniformity is in contrast with spheroids derived from unsorted cells, which displayed a more heterogeneous growth pattern, with a mean diameter of 203.20 ± 102.93 μm by Day 35. Statistical analysis using an unpaired *t*-test with unequal variances confirmed that this difference in spheroid size is significant, with a p-value of 0.0417 ($p < 0.05$).

These findings demonstrate that CSC-derived spheroids, when cultured in a well-defined hydrogel, exhibit highly reproducible growth patterns compared to spheroids derived from unsorted cells, making them a more reliable 3D model for biological research and drug testing applications.

1. Introduction

Cell culture is a fundamental method used in a wide variety of applications, notably in biological and medical research. For example, cell culture is proving very useful in drug therapy trials and drug design in personalized medicine including the study of the impact of therapeutic nanoparticles as drug vectors, in regenerative medicine, for stem cells studies and in oncology research to understand cancer progression [1-5]. The last decade has seen a shift from applying conventional two-dimensional (2D) cell culture to the use of three-dimensional (3D) cell culture. 3D cell culture enables the recapitulation of realistic cellular morphology, cell-to-cell and cell-to-matrix interactions *in vivo* [6,7]. In cancer research, for example, 3D models consisting of cancer cells present in a 3D scaffold enable the physico-chemical properties of the physiological extracellular matrix (ECM) to be mimicked [5]. As a result, cancer cells behave in the same way as *in vivo, i.e.* they develop into

* Corresponding authors.
E-mail addresses: bruno.alies@inserm.fr (B. Alies), serge.battu@unilim.fr (S. Battu).
[1] These authors contributed equally to the paper as first authors.

https://doi.org/10.1016/j.chroma.2024.465393
Received 16 July 2024; Received in revised form 19 September 2024; Accepted 21 September 2024
Available online 22 September 2024

multicellular tumor spheroids (MCTS) representative of solid tumors [8, 9]. Thus, applications of 3D models are on the increase and are becoming an alternative to the use of animal models, which present numerous challenges such as ethical, financial and scientific controversies [5].

Several culture methods have been developed to produce 3D tumor spheroid models such as suspended droplets [10,11], rotating flask or rotating cell containers [12,13] and so on. Nevertheless, these methods have very low spheroid generation yields and high variability in spheroids size and morphology. Consequently, they have been replaced by more efficient approaches such as ultra-low attachment plates, microfluidic systems, microarrays, etc. [14-16]. Although these methods enable the generation of spheroids of uniform size, they still present technical challenges in terms of handling, maintenance, uniformity and automation; consequently, post-culture assays cannot be easily performed. It should also be noted that all these studies focus on 3D culture methods to achieve reproducibility of size and morphology, and not on the nature of the cell model itself. Implementing a homogeneous cell population with specific tumor-initiating properties could help overcome these obstacles. In fact, cancer stem cells (CSCs) are a very rare subpopulation found in cancer cell lines in low proportions (1–5%) [17]. CSCs possess two essential characteristics: their high capacity for self-renewal, also defined by a low proliferation rate, and their multipotency, which gives rise to a phenotypically heterogeneous subset of cells [18-20]. They play a key role in tumorigenesis processes [21] due to their ability to initiate and sustain tumor development [22] and because they are the main cause of drug resistance [23]. Consequently, CSCs are known as tumor initiating cells [24]. They are therefore good candidates for cell culture aimed at developing reproducible spheroids particularly with regard to growth kinetics and size [21]. In that way, we purpose to routinely prepare the CSCs subpopulation by using sedimentation field-flow fractionation (SdFFF). Among the FFF family, SdFFF have been historically used for eukaryotic cell sorting [25]. The separation takes place in an empty ribbon-like separation channel (no stationary phase), where cell species are submitted to two types of forces (1) hydrodynamic lift forces generated by flowing a carrier liquide through the channel and (2) a multigravitational external field applied perpendicularly to the flow direction. The main advantage in cell sorting is the limitation of cell/cell interactions, or cell/surface interaction by using the empty separation channel and by enhancing a pure hyperlayer elution mode [25-27]. In that case, cells reach their equilibrium position where the multigravitational external field is counterbalanced by hydrodynamic lift forces [28], leading to cell elution above the accumulation wall, and to reduce harmful interactions. This equilibrium position only depends on the intrinsic biophysical properties of cells such as diameter, density, and in a less extend, shape and rigidity [28]. Then, according to the hyperlayer elution mode, large cells elute first, denser cells last. Because these biophysical properties are intrinsically linked to biological ones, this makes SdFFF a gentle, fast, effective and label free cell sorting method [26,29-32], particularly well-suited to CSC subpopulation sorting from glioblastoma cell lines [27,33,34].

Cell culture in a 3D scaffold made from biomaterials such as hydrogels has also attracted a great deal of interest due to the physicochemical properties of hydrogel. Unfortunately, it has become clear that the use of uncontrollable natural biomaterials such as Matrigel will not provide a reproducible model due to the intrinsic variability of biomaterial such as batch-to-batch and within batch chemical irregularities [35]. In addition, it is important that the 3D scaffold meets key characteristics such as the retention of an ECM-like fibrillar structure and ease of handling for testing in subsequent experiments. Low Molecular Weight Gelators (LMWGs) consist of small molecules that undergo supramolecular self-assembly to form a hydrogel based on weak interactions, an important feature for reversibility and tunable physical characteristics [5,36]. Among LMWGs, Glycosyl-nucleo-bola-amphiphile (GNB) which possesses two amide groups (called later BA from Bis-Amide) [37,38] has been used previously and proved effective for 3D culture [39]. From a practical standpoint, the gelation kinetics allow easy manipulation of the gel during a 3D culture experiment. In addition, the porous structure of this hydrogel enables molecular mobility of particles such as nutrients and proteins that are mandatory for 3D culture process and analysis [39]. This biomimetic architecture features controlled chemical composition and viscoelastic properties compared to the Matrigel approach. LMWGs are therefore good candidates for cell culture aimed at developing spheroids with the desired reproducible characteristics.

Accordingly, in this study, we sought to achieve, for the first time, a 3D culture of CSCs derived from a cancer cell line in a supramolecular hydrogel. With this cell-hydrogel combination, we hoped to perform 3D models in which spheroids of uniform-size would be obtained. Heterogeneous glioblastoma (GBM) cell line (U87-MG) was selected because of its specific CSC content and our ability to sort them by using calibrated SdFFF cell sorting [27,34]. SdFFF elution provides two different populations, a sub-population of differentiated cells and another of CSCs that were implemented in LMWG GNB hydrogel, compared with unsorted cells.

2. Material and methods

A Schematic representation of the 3D culture process is presented in Fig. 1.

2.1. Cell culture

The human glioblastoma cell line U87-MG was purchased from the American Type Culture Collection (ATCC, Manassas, VA, USA) and grown in Gibco Dulbecco's Modified Eagle Medium cell medium (DMEM), 10% fetal bovine serum (FBS), 1% non-essential amino acids and 1% penicillin/streptomycin. Cells were cultured at 37 °C in a 5% CO_2 incubator with 20% O_2. After culture time, cells are dissociated using Versene solution (Thermofisher scientific, France) and centrifuged at 300 g for 5 min. Cells are then resuspended with DMEM and counted using trypan blue (Sigma) exclusion and Malassez cell counting chamber.

2.2. SdFFF device and cell elution conditions

The SdFFF separation device used in this study was previously described. [27,34]. The apparatus consisted of two 880 × 47 × 2 mm3 polystyrene plates separated by a Mylar® spacer into which a channel was carved. The channel had dimensions of 788 × 12 × 0.175 mm3, with two 50 mm V-shaped ends. The measured total void volume (channel volume + connecting tubing + injection/detection device) was 1906 ± 10.00 µL (n = 6). Void volume was calculated after determination of elution time of a non-retained compound (0.10 g/L benzoic acid, UV detection at 254 nm). The channel rotor axis distance was r = 14.80 cm. Sedimentation fields were expressed in units of gravity, 1 g = 980 cm/s^2. A T90S2 asynchronous motor (Brown Group, Limas, France) was connected to a COMBIVERT F4 pilot unit (Keb, La Queue en Brie, France) [40]. An LC-20AD UPLC pump (Shimadzu, Champ/Marne, France) was used to pump the sterile mobile phase. Sample injections were performed using a Rheodyne ® 7125i chromatographic injector (Rheodyne, Cotati, CA, USA). The elution signal was recorded at 254 nm on a SPD-20AV UV/VIS Detector (Shimadzu) with a NI9211 (10 mV input) acquisition device (National Instruments France, Nanterre, France) operated at 3 Hz and connected to a personal computer controlled by Visual Basic software developed in-house (VB pro, Ver 6.0, Microsoft Corp.).

Optimal elution conditions were as follows: flow administration through the accumulation wall of a 100 µL U87-MG cell suspension (2.10^6 cells/mL). Flow rate: 1.0 mL/min. Carrier liquid: sterile Dielectrophoresis (DEP) buffer (osmotic sucrose-based survival buffer [34]), pH 7.4 and conductivity 24mS/m. External multigravitational field strength: 15 g for U87-MG. Time dependent fraction collection (Fig. 2):

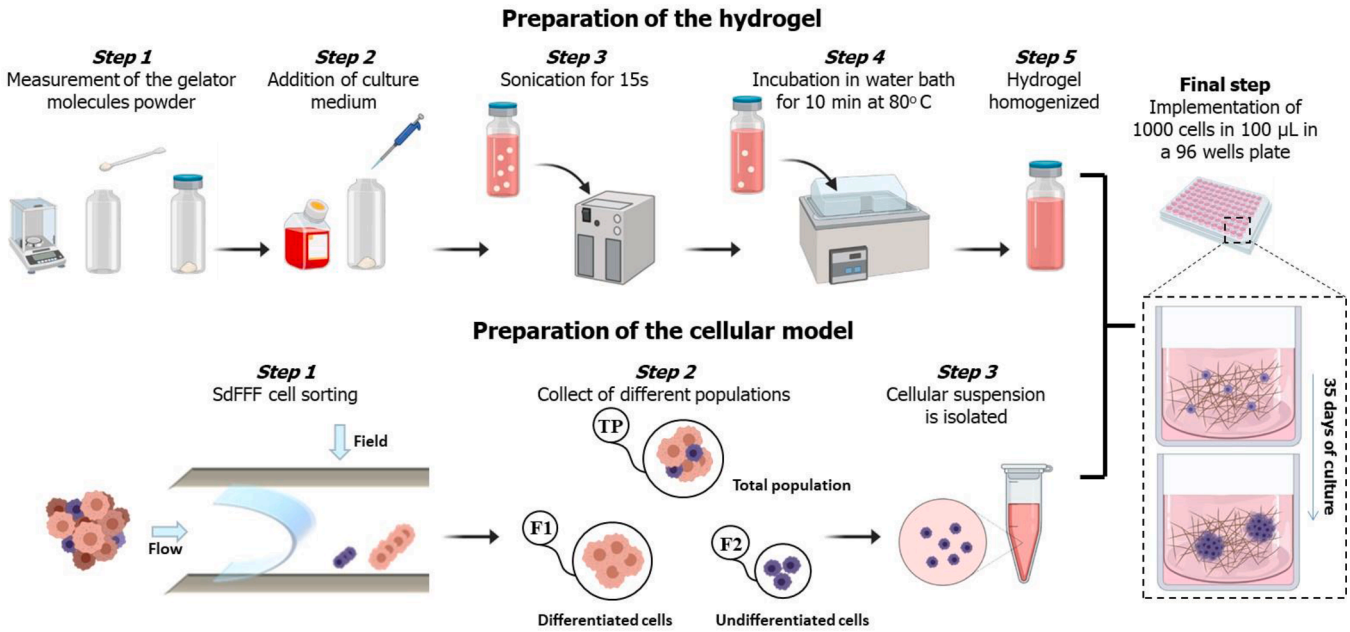

Fig. 1. Schematic representation of the 3D culture process from the production of the hydrogel to the formation of tumor spheroids, with the steps of gel preparation, cell sorting and final implementation of the cells into the hydrogel.

Differentiated cells Fraction 1 (F1): 2 min 35 s to 4 min 20 s; CSCs Fraction 2 (F2): 6 min 2 s to 8 min 5 s. And total peak (TP, as a control) which constitutes the collection of the entire eluted population (except the void volume): 2 min 35 s to 8 min 5 s. The crude population constitutes the remaining unsorted cells suspension of the experiment. In order to obtain enough cells for further analysis and subculture, consecutive (10 - 12 injections) SdFFF fraction collections were performed and the variation of the retention ratio ($R_{obs} = t_0/t_R$ [7,41]) provides RSD < 5%.

2.3. 3D cell culture

The hydrogel is formed by adding an adequate volume of cell culture medium (DMEM+FBS) on a specific mass of powder of Glycosyl-nucleobola-amphiphile (GNB) with two amide groups (GNB-BA for Bis-Amide) in order to get the concentration desired. The structure of GNB-BA is given in Figure S.1. For a concentration of 0.25% w/v, 1000 µL of cell medium are added on 2.5 mg of gelator powder. The mixture is then sonicated for 15 s and placed in a water bath at 80 °C for 10 min to ensure complete solubilization. Then, the mixture is cooled down at room temperature before a cell suspension of 1000 cells per 100 µL is prepared and mixed with the BA in their sol phase. Previous data have shown that BA 0.25% w/v remains in sol phase for 7 min after solubilization at room temperature before undergoing gelation [39]. The suspension is homogenized within the final mixture and distributed in a 96 wells plate (100 µL per well). Once the gelation process is over, 200 µL of cell culture medium is added to each well and the plate is incubated for a month and cell medium is changed every 48 h. Cell culture is examined for 35 days because a growth threshold is observed at this time.

For the 3D culture of F2 sub-population, three different repetitions of experiment at different days are conducted: each experiment consists of a cell sorting by SdFFF and a preparation of BA 0.25% w/v hydrogel, and the cells are then implemented in three wells of a 96 wells plate.

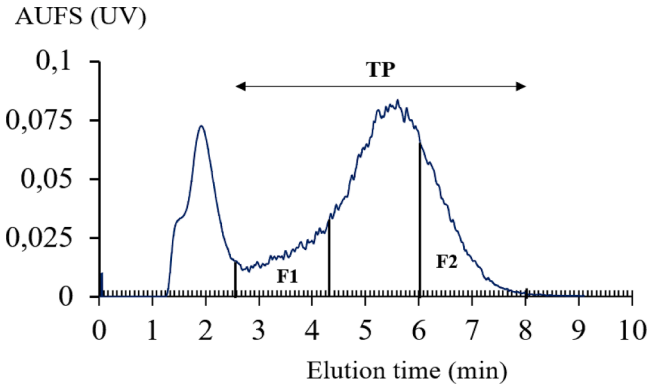

Fig. 2. Representative SdFFF fractogram of U87-MG cell line. Elution conditions: flow rate of sterile PBS (ph 7.4) 1.0 mL/min; external gravitational field 15 g; Y-axis is absorbance unit full scale (AUFS) of a spectrophotometric detection at 254 nm. Injection of 100 µL of cell suspension (2×10^6 cell/mL). Time dependent fraction collection: differentiated cells = Fraction 1 (F1); CSCs = Fraction 2 (F2); Total peak (TP) = control.

2.4. Cellular characterization

Reverse Transcription quantitative Polymerase Chain Reaction (RTqPCR): RNA isolation from cells was performed with RNeasy Mini Kit (# 74,106; QIAGEN, Germany). After quantification, 2 µg of total RNA was reverse transcribed with a high-capacity cDNA Reverse Transcription Kit (Applied Biosystems). qPCRs on 100 ng of cDNA were performed with Premix Ex Taq™ (#RR39WR, TaKaRa®) on QuantStudio 3 real-time thermal cycler (Applied Biosystems) with TaqMan™ probes for each reaction. Probes used for quantitative RT-qPCR are listed in Table SI-1. Reactions were performed in triplicate from each biological replicate. Relative gene expression was quantified using Glyceraldehyde-3-phosphate dehydrogenase (GADPH) as house-keeping gene. The ΔΔCt quantitative method was used to normalize expression of the reference gene and to calculate the relative expression levels of target genes. Probes used for quantitative RT-qPCR were purchased from Thermofisher France: GAPDH (Hs02758991_g1), NANOG (Hs02387400_g1), POU5F1 (Oct4; Hs00999634_gH) and SOX2 (Hs01053049_s1).

Live/dead assay: Cell viability assessed by a fluorescent viability/cytotoxicity assay (Thermofisher scientific, France). Live cells fluoresce green due to the uptake and fluorescence of calcein-AM in response to

intracellular esterase activity; dead cells fluoresce red as a result of the entry of ethidium homodimer-1 through damaged cell membranes and subsequent binding to nucleic acids. Cells were then imaged using LEICA DMi8 microscope.

Growth kinetics: In order to evaluate tumor growth over time, growth kinetics were studied by measuring tumor diameters at different timepoints using ImageJ software. Mean size and standard deviations are presented for each timepoint of the culture (day 5, 15, 25 and 35) that were measure on different culture assays to represent repeatability or lack thereof.

MTT assay: MTT assay is used to evaluate cellular metabolic activity at different timepoints of a 35 days culture. Preexistent culture medium, that formed the supernatant above the gel, is discarded and replaced with 100 μL of culture medium slowly without disturbing the gel. Then, 20 μL of MTT solution are added to each well and the plate wax incubated for 4 h. Afterwards, 100 μL of mixture is extracted from each well to a new 96 wells plate and absorbance was read at 492 nm using a plate reader.

Immunofluorescence: Isolated spheroids are embedded in OCT, and cryo-sectioned in 4 μm sections via an ultramicrotome. Sections are then stained with an anti-ki67 marker (sigma) overnight and DAPI for 15 min and observed using LEICA DMi8 microscope.

Confocal microscopy imaging: Isolated spheroids are acquired by manual removal using scalpel alongside pipette tip cone. They are then fixed using paraformaldehyde 4% and then washed with PBS on a glass slide at room temperature. Calceine-AM was then added for 1 hour. To avoid disturbing the architecture of the spheroid, there is no addition of a small glass slide on top. Then the spheroid is imaged using Zeiss LSM 880.

2.5. Statistical analysis

Statistical analysis was performed on three independent experiments of cell cultures, fractions and characterization using Prism GraphPad software. Analysis of variance (ANOVA), Student's *t*-test, and Mann−Whitney test were conducted to compare different conditions. P values ≤ 0.05 were considered statistically significant.

3. Results and discussion

3.1. Cell sorting from a GBM cell line

As previously described, heterogeneous Glioblastoma cell line (U87-MG) is routinely sorted by SdFFF [31,32]. The SdFFF hyperlayer cell sorting [26,27,34] generate different populations (Fig. 2): Fraction 1 (F1) constituting the differentiated cells sub-population and Fraction 2 (F2) constituting the CSCs sub-population. Post SdFFF cell integrity was monitored by collecting the total peak (TP) (Fig. 2). Comparison of the TP population obtained by SdFFF sorting and unsorted cells referred to as crude sample shows the same phenotypical and functional characteristics, enabling this TP to be used as a control. In agreement with our previous study, and to routinely validate the quality of this process, we systematically analyze our cell subpopulations. Systematic characterization was performed on all the fractions, gene expression assessment at transcriptomic level by RTqPCR was performed by measuring the expression of intracellular and intranuclear transcription factors Oct4, Sox2 and Nanog (Figure S.2), that are considered as key CSCs markers [27,34,42-45]. This result shows a differential analysis of CSCs mRNA expression levels, assessed in F1 and F2 sub-populations for the U87-MG cell line. All three CSCs markers (Oct4, Sox2 and Nanog) are significantly overexpressed in F2 compared to F1: 3.3 times more in F2 than in F1 for Oct4, 3 times more in F2 than in F1 for Sox2 and 4.9 times more in F2 than in F1 for Nanog. These results are consistent with previous findings [34]. Furthermore, no significant differences were observed between TP and crude sample. Therefore, after cell sorting by SdFFF, the two sub-populations of interest: F1 a sub-population of differentiated cells and F2 a sub-population of CSCs were implemented in the GNB-BA 0.25% w/v hydrogel (see chemical structure of the single molecule that forms the hydrogel in Figure S.1) to study their behavior in 3D culture.

3.2. Three-dimensional culture of cells sorted by SDFFF

We previously examined the behavior of glioblastoma cancer cell line, U87-MG, in 3D culture and observed a production of spheroids with heterogeneous shapes and sizes [39]. Therefore here, we evaluated the 3D culture of the TP control population and the sub-populations acquired after SdFFF cell sorting (F1 differentiated and F2 undifferentiated).

First, we examined as a control, the 3D culture of the TP population (Fig. 2) which consists of the collection of all cells from injection in SdFFF, making it a heterogeneous population with cells of all stages of differentiation analogous to unsorted U87-MG (crude sample) that have been tested previously [39]. Fig. 3A shows the 3D culture of the TP population which was able to proliferate and maintained high viability throughout the culture period. To complete the picture, Figure S.3 shows five different 3D cultures of the TP population from three different cell sorting experiments and three different hydrogel batches. We observed highly stochastic cellular behavior with very different growth kinetics resulting in spheroids between 50 and 300 μm in size after 35 days of culture. Spheroids of 10 to 200 μm were observed when the unsorted GBM cell line was cultured [39]. Similar behavior were observed between unsorted cells and the TP population but the results lacked uniformity in terms of size and morphology.

Secondly, the F1 fraction which consists of a sub-population enriched in differentiated cells was examined in 3D culture. Due to the absence of stemness properties (self-renewal and multipotency), differentiated cells were not expected to generate tumor [27,34,46,47]. Fig. 3B shows the 3D culture of the undifferentiated F1 fraction sorted by SdFFF in GNB-BA 0.25% w/v exhibiting only viable cells throughout the 35 days of culture with no proliferation reported. Furthermore, Figure S.4 shows F1 repeated cultures from three different cell sorting experiments and three different hydrogel batches. We interestingly observed that when F1 was implemented in hydrogel, the cells are unable to proliferate or organize into tumor spheroids but remain viable until day 35.

Thirdly and in an original manner, we evaluated the behavior and development of the F2 sub-population in GNB-BA 0.25% w/v. F2 is a population of CSCs sorted by SdFFF, known for being tumor-initiating cells [17,18,21,22,24]. We observed a high viability of the cells in the gel throughout the culture time from day 5 until day 35 (Fig. 4A). The 3D culture of the F2 population from three different cell sorting experiments and hydrogel batches is showed in Fig. 4B. This demonstrates the reproducibility of spheroid production. Moreover, the spheroids generated with F2 are larger than those produced with TP and therefore more representative of solid tumors *in vivo*.

In addition, image analysis of TP repeated cultures is illustrated in Fig. 5A Top. Five curves are shown, each reflecting a culture of a TP population in the GNB-BA 0.25% w/v from day 5 to day 35 with. This result shows a highly variable evolution of the growth kinetics of heterogeneous TP cells over culture time. Furthermore, box plots show a broad distribution of spheroid size for each time point with large standard deviation (Fig. 5A), demonstrating the lack of repeatability of the experiment with a mean of 203 μm and a standard deviation of 103 μm on day 35.

On the other hand, image analysis of F2 repeated cultures is shown in Fig. 5B. Nine curves are shown, each reflecting a culture of an F2 population in the GNB-BA 0.25% w/v from day 5 to day 35. We observed a repeated evolution of size between all the individual cultures, the superposition of the nine curves proving the repeatability and reproducibility not only of the spheroids generated by the end of the culture, but also of the evolution of size throughout the duration of the culture. In particular, an interesting observation was made between day 25 and day 35, showing a significant increase in tumor size. This is indicative of

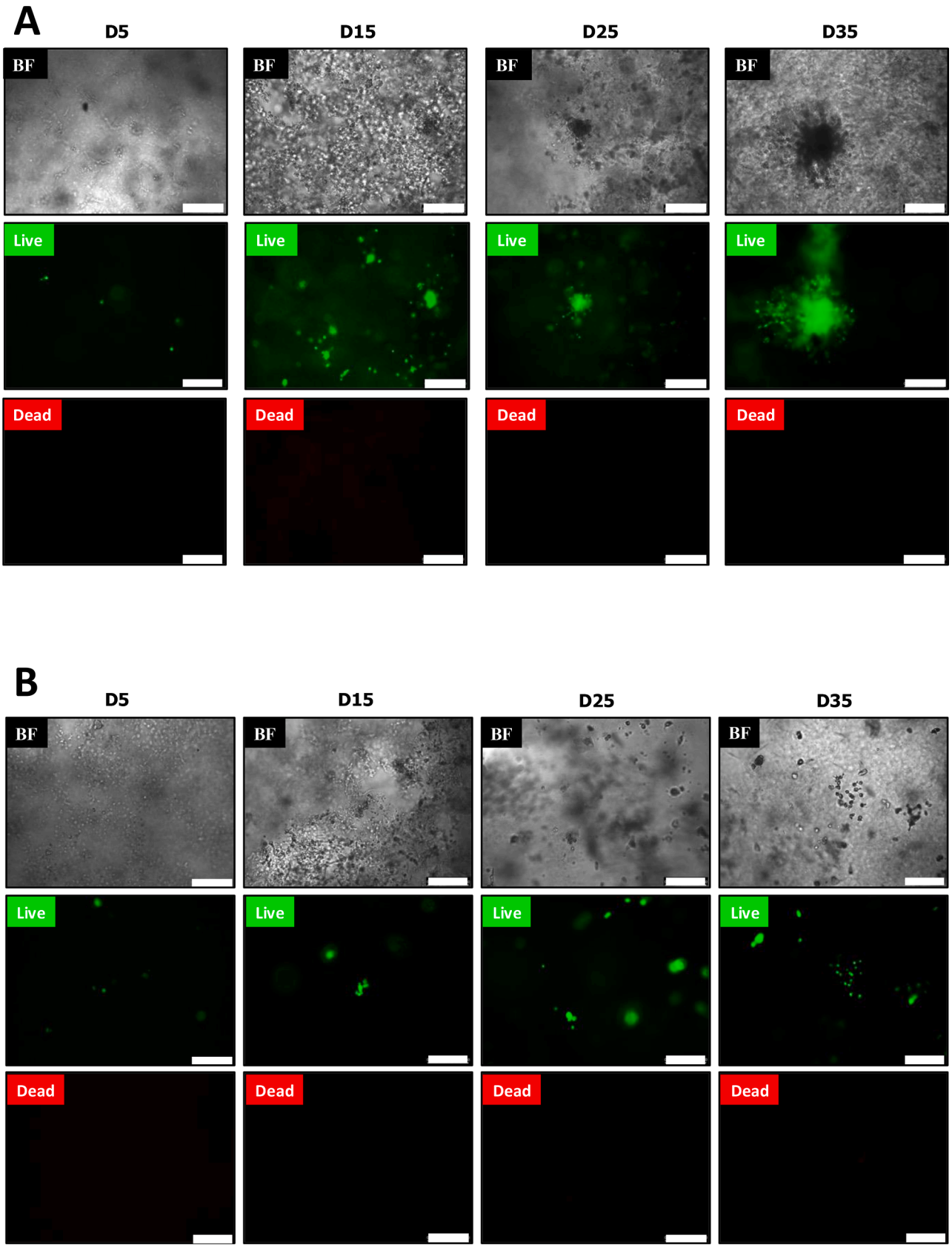

Fig. 3. 3D culture of TP (**A.**) and F1 (**B.**) after SdFFF in GNB-BA 0.25% w/v over 35 days (D5 = day 5; D15 = day 15; D25 = day 25; D35 = day 35). Top panel represents bright field (BF) imaging, middle and bottom panels represent imaging using the Live/Dead kit to assess live cells with calcein-AM dye (green) and dead cells using ethidium homodimer-1 dye (red) (See Material and Methods section). Scale bar = 250 μm.

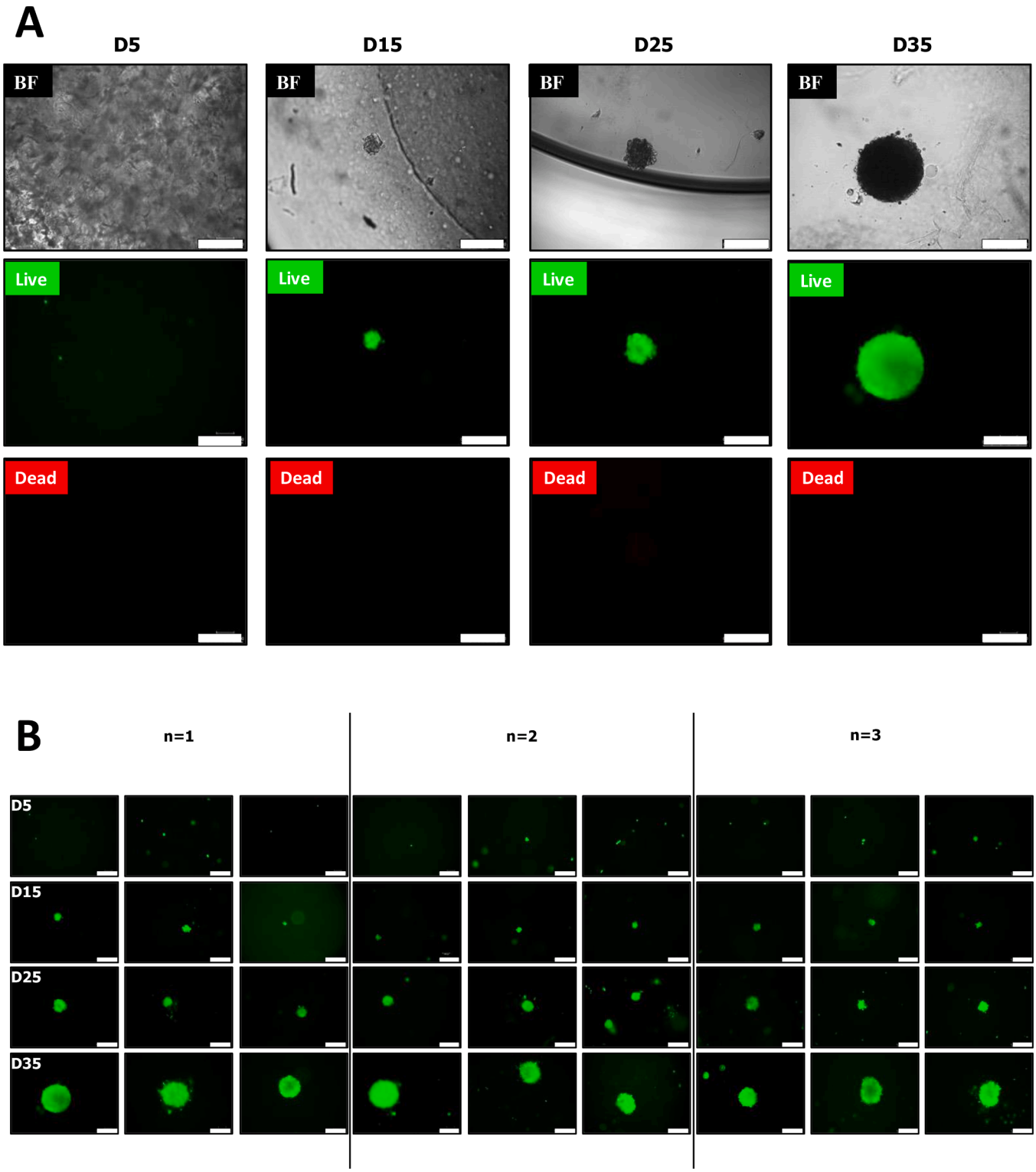

Fig. 4. 3D culture of SdFFF F2 cells in GNB-BA 0.25% w/v over 35 days (D5 = day 5; D15 = day 15; D25 = day 25; D35 = day 35). **A** (top panels) Example of 3D culture of SdFFF F2 cells. Top panel represents bright field (BF) imaging, middle and bottom panels represent imaging using the Live/Dead kit to evaluate the live cells with calcein-AM (see Materials and Methods section). **B.** (bottom panels) Chronology of 3 different 3D cultures of the F2 U87-MG sub-population (n = 1 to 3) from day 5 to day 35 represented by fluorescent imaging using calcein-AM dye showing the production of uniformly sized spheroids from CSCs (3 replicates from independent experiments). Scale bar = 250 μm.

healthy cell growth and active spheroid dynamics resulting in large and viable MCTS for each culture, representative of tumors *in vivo*. In addition, the box plots (Fig. 5B) show the spheroid size distribution for each time point with a standard deviation smaller than of the TP, proving the repeatability of the experiment as a consequence of the homogeneity of the population. Thus, by implementing 1000 CSCs cells per well in our 3D system, we were able to generate reproducible tumor spheroids of uniform size with a mean of 350 μm and a standard

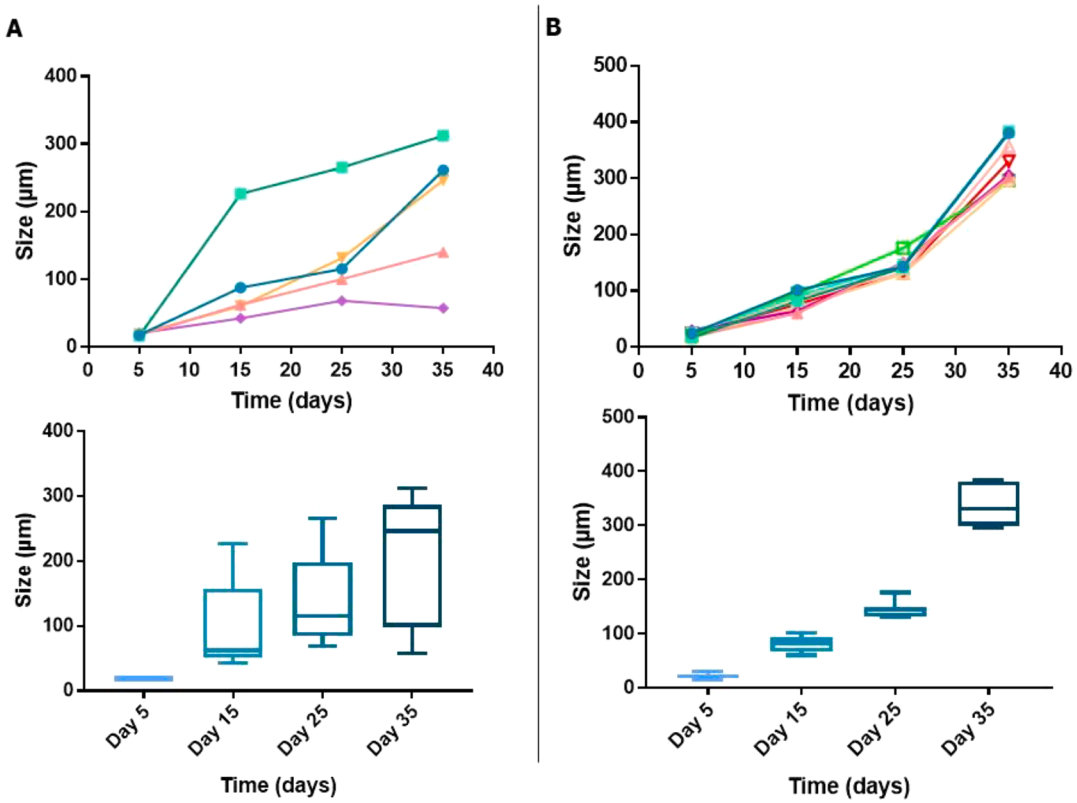

Fig. 5. Evaluation growth kinetics of U87-MG TP (**A** left panel) and F2 (**B** right panel) population grown in GNB-BA 0.25% w/v assessed over a 35-day period by ImageJ software analysis. Data represent the mean cell growth of each TP (**A** left panel) or F2 (**B** right panel) culture and their associated box plots showing spheroid size distribution.

deviation of 30 µm (less than 10% RSD).

In summary, the calculated mean diameter of 336.67 ± 38.70 µm for CSC-derived spheroids on Day 35 reflects a tight distribution around the mean, indicating that the 3D culture of CSCs in the hydrogel produces spheroids of reproducible size. In contrast, unsorted cells formed spheroids with a mean diameter of 203.20 ± 102.93 µm, with a larger standard deviation, suggesting greater variability in their growth. Finally, the unpaired *t*-test (Welch's test) yielded a p-value of 0.0417, confirming that the difference in spheroid sizes between CSC-derived spheroids and unsorted cell-derived spheroids is statistically significant ($p < 0.05$).

Overall, comparative analysis of the 3D culture of TP, F1 and F2 proves that (1) reproducible tumor spheroids in terms of evolution and uniformity are strongly depend of the homogeneity of the population implemented; (2) taking into account the nature of the cell model rather than 3D culture method could be a good trajectory for achieving reproducibility and (3) CSCs which are known to be tumor-initiating cells *in vivo,* are the only population capable of generating large, viable spheroids of uniform size.

3.3. *Spheroid validation by comparative analysis of the metabolic activity of 3D cultures obtained from different subpopulations sorted by SDFFF*

During tumor progression, cells adapt their metabolic activity to cope with their proliferation rates. CSCs are known to have a distinct metabolic phenotype dependent on high glycolytic activity as well as high oxidative phosphorylation. Differentiated cells on the other hand depend mainly on glycolysis [48]. This is correlated with the proliferation and growth behavior previously observed. To highlight the difference in metabolic activity between populations in 3D culture, we performed an MTT assay (Fig. 6) showing the metabolic activity of cells after SdFFF, which is approximatively proportional to cell proliferation.

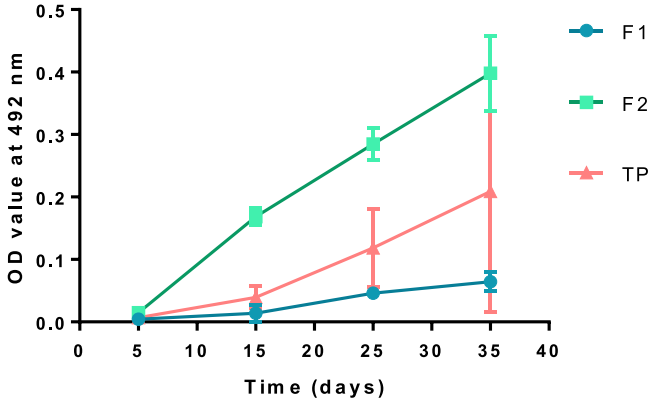

Fig. 6. Comparison of the metabolic activity of TP, F1 and F2 during 3D culture in GNB-BA 0.25% w/v function of time (days) using the MTT assay. Optical Density (OD) values measured at 492 nm.

We observed that the CSCs (F2) population showed an increase in metabolic activity from day 5 to day 35 with minimal standard deviation and recorded the highest metabolic at day 35 among the three populations. We can conclude that this increase in metabolic activity is due to the reproducible growth of spheroids. (Fig. 5B)

The TP population also showed an increase in metabolic activity but with great variability between cultures as illustrated by the large standard deviation. Indeed, we observed that some TP cultures showed active proliferation while others remained only viable. This can be explained by the various cell types contained in the TP (differentiated cells, CSCs precursors and CSCs), reflecting the heterogeneity of glioblastoma. While the differentiated cells (F1), showed relatively low and constant metabolic activity throughout culture. This is due to the small,

but viable, number of cells observed from day 5 to day 35.

These findings underline the importance of using SdFFF-sorted CSCs in 3D culture, in order to obtain a reproducible result regarding viability, proliferation, organization and metabolic activity. They also highlight that *in vitro* 3D CSCs models are very important as they generate a platform containing spheroids that are representative of solid tumors *in vivo*. However, further characterization is needed to conclude that the internal spheroid structure is also representative of GBM tumors.

3.4. Characterization of spheroids specially produced by glioblatoma CSCs

GBM spheroids grown cultures in a 3D system should present different layers of cells, with an outer layer composed of proliferative cells, an intermediate layer composed of quiescent cells and the inner core where CSCs predominantly reside is hypoxic and necrotic [49-52] To demonstrate the multicellular aspect of the spheroids obtained, we performed an immunostaining on a spheroid section. We assessed that Ki67 expression, a marker highly expressed in proliferative cells. In Figure S.5, we can see that Ki67 expression forms an intensity gradient with a peak at the membrane and lower intensity at the core. This result shows that peripheral cells are highly proliferative while core cells are less so.

Next, to assess the spatial organization of the spheroid, we performed confocal microscopy on an isolated spheroid using Calcein-AM staining. Image J software analysis of the image showed construction at different z-axis levels, demonstrating the three-dimensional positioning of the spheroid within the hydrogel (Figure S.6). This characterization of spheroids shows that hydrogel enables 3D construction of the biological system with a viable outer layer and a necrotic core.

4. Conclusion

The successful design of a 3D model such as MCTS relies on two key compounds, a 3D scaffold and a cellular model, which must be perfectly defined and mastered. In this study, a hydrogel, obtained by the supramolecular self-assembly of singles molecules (low molecular weight gelators), was used as a controlled 3D scaffold. The viscoelasticity of the 3D scaffold is controlled by adjusting the concentration of gelator molecules to match the environment of the chosen cell line. It should noted that the concentration is low enough to produce a large volume of hydrogel at low cost. Gelling kinetics are compatible with cell processing, being fast enough to prevent cell sedimentation but slow enough to facilitate their internalization into the gel. This 3D scaffold mimics the architecture of the extracellular allowing the cell model to develop into a multicellular tumor spheroid. However, reproducibility of 3D systems remains one of the greatest challenges. In fact, to be reliably used for different types of applications, a 3D model must always be able to provide the same starting point of analysis. In other words, the 3D model should ideally always be produced with the same biophysical characteristics. Implementing a cancer stem cells population of in GNB-BA 0.25% w/v hydrogel overcame these difficulties. Indeed, on the on hand, CSCs possess key characteristics, such as self-renewal and multipotency, which enable them to initiate tumor development *in vivo*, and form solid tumors from a small number of cells. On the other hand, cell sorting of GBM cell lines (U87-MG) by SdFFF enables the isolation of sub-populations of CSCs, without impairing their intrinsic biological properties. The results of the 3D culture of SdFFF sub-populations demonstrate that CSCs generate reproducible production of spheroids of uniform size, high viability, repeatable growth kinetics and spatial organization. In contrast, the sub-population of differentiated cells was enable to generate any cell growth during 35 days of culture and the heterogeneous population generated heterogeneous MCTS. Consequently, CSCs are required to achieve high reproducibility of morphology and size. However, the three-dimensional structure of the spheroids needs to be further characterized to better highlight the different layers and their transcriptomic profiles.

Finally, the reproducibility of this system, particularly at different time of culture, means that it can be used in a wide variety of applications.

CRediT authorship contribution statement

Tarek Saydé: Writing – review & editing, Writing – original draft, Methodology, Investigation. **Omar El Hamoui:** Writing – review & editing, Methodology, Investigation. **Bruno Alies:** Writing – review & editing, Supervision, Methodology, Funding acquisition, Formal analysis, Conceptualization. **Gaëlle Bégaud:** Writing – review & editing, Methodology, Investigation. **Barbara Bessette:** Methodology, Investigation. **Sabrina Lacomme:** Methodology, Investigation, Formal analysis. **Philippe Barthélémy:** Writing – review & editing, Supervision, Project administration, Conceptualization. **Gaëtane Lespes:** Writing – review & editing, Supervision, Resources, Project administration, Methodology, Funding acquisition, Formal analysis, Conceptualization. **Serge Battu:** Writing – review & editing, Validation, Supervision, Resources, Methodology, Funding acquisition, Formal analysis, Conceptualization. **Karen Gaudin:** Writing – review & editing, Supervision, Resources, Project administration, Methodology, Formal analysis, Conceptualization.

Declaration of competing interest

The authors declare that they have no known competing financial interests or personal relationships that could have appeared to influence the work reported in this paper.

Data availability

The authors do not have permission to share data.

Acknowledgements

This study was supported ‘’Région Nouvelle Aquitaine’’ (3D Strom project: 2018-1R10128) and the "Ligue Contre le Cancer Comité de la Gironde".

Supplementary materials

Supplementary material associated with this article can be found, in the online version, at doi:10.1016/j.chroma.2024.465393.

References

[1] K. Duval, H. Grover, L.H. Han, Y. Mou, A.F. Pegoraro, J. Fredberg, Z. Chen, Modeling Physiological Events in 2D vs. 3D Cell Culture, Physiology 32 (2017) 266–277.
[2] R. Edmondson, J.J. Broglie, A.F. Adcock, L.J. Yang, Three-Dimensional Cell Culture Systems and Their Applications in Drug Discovery and Cell-Based Biosensors, Assay Drug Dev. Technol. 12 (2014) 207–218.
[3] C. Jensen, Y. Teng, Is It Time to Start Transitioning From 2D to 3D Cell Culture? Front. Mol. Biosci. 7 (2020).
[4] M. Ravi, V. Paramesh, S.R. Kaviya, E. Anuradha, F.D.P. Solomon, 3D Cell Culture Systems: Advantages and Applications, J. Cell. Physiol. 230 (2015) 16–26.
[5] T. Sayde, O. El Hamoui, B. Alies, K. Gaudin, G. Lespes, S. Battu, Biomaterials for Three-Dimensional Cell Culture: From Applications in Oncology to Nanotechnology, Nanomaterials 11 (2021).
[6] Y. Imamura, T. Mukohara, Y. Shimono, Y. Funakoshi, N. Chayahara, M. Toyoda, N. Kiyota, S. Takao, S. Kono, T. Nakatsura, H. Minami, Comparison of 2D-and 3D-culture models as drug-testing platforms in breast cancer, Oncol. Rep. 33 (2015) 1837–1843.
[7] M. Kapalczynska, T. Kolenda, W. Przybyla, M. Zajaczkowska, A. Teresiak, V. Filas, M. Ibbs, R. Blizniak, L. Luczewski, K. Lamperska, 2D and 3D cell cultures - a comparison of different types of cancer cell cultures, Arch. Med. Sci. 14 (2018) 910–919.

[8] F. Hirschhaeuser, H. Menne, C. Dittfeld, J. West, W. Mueller-Klieser, L.A. Kunz-Schughart, Multicellular tumor spheroids: An underestimated tool is catching up again, J. Biotechnol. 148 (2010) 3–15.

[9] R.M. Sutherland, Cell and environment interactions in tumor microregions - The multicell spheroid model, Science 240 (1988) 177–184.

[10] G. Mehta, A.Y. Hsiao, M. Ingram, G.D. Luker, S. Takayama, Opportunities and challenges for use of tumor spheroids as models to test drug delivery and efficacy, J. Control. Release 164 (2012) 192–204.

[11] P. Sabhachandani, V. Motwani, N. Cohen, S. Sarkar, V. Torchilin, T. Konry, Generation and functional assessment of 3D multicellular spheroids in droplet based microfluidics platform, Lab Chip 16 (2016) 497–505.

[12] J. Friedrich, R. Ebner, L.A. Kunz-Schughart, Experimental anti-tumor therapy in 3-D: Spheroids - old hat or new challenge? Int. J. Radiat. Biol. 83 (2007) 849–871.

[13] P. Godoy, N.J. Hewitt, U. Albrecht, M.E. Andersen, N. Ansari, S. Bhattacharya, J. G. Bode, J. Bolleyn, C. Borner, J. Bottger, A. Braeuning, R.A. Budinsky, B. Burkhardt, N.R. Cameron, G. Camussi, C.S. Cho, Y.J. Choi, J.C. Rowlands, U. Dahmen, G. Damm, O. Dirsch, M.T. Donato, J. Dong, S. Dooley, D. Drasdo, R. Eakins, K.S. Ferreira, V. Fonsato, J. Fraczek, R. Gebhardt, A. Gibson, M. Glanemann, C.E.P. Goldring, M.J. Gomez-Lechon, G.M.M. Groothuis, L. Gustavsson, C. Guyot, D. Hallifax, S. Hammad, A. Hayward, D. Haussinger, C. Hellerbrand, P. Hewitt, S. Hoehme, H.G. Holzhutter, J.B. Houston, J. Hrach, K. Ito, H. Jaeschke, V. Keitel, J.M. Kelm, B.K. Park, C. Kordes, G.A. Kullak-Ublick, E.L. LeCluyse, P. Lu, J. Luebke-Wheeler, A. Lutz, D.J. Maltman, M. Matz-Soja, P. McMullen, I. Merfort, S. Messner, C. Meyer, J. Mwinyi, D.J. Naisbitt, A. K. Nussler, P. Olinga, F. Pampaloni, J.B. Pi, L. Pluta, S.A. Przyborski, A. Ramachandran, V. Rogiers, C. Rowe, C. Schelcher, K. Schmich, M. Schwarz, B. Singh, E.H.K. Stelzer, B. Stieger, R. Stober, Y. Sugiyama, C. Tetta, W.E. Thasler, T. Vanhaecke, M. Vinken, T.S. Weiss, A. Widera, C.G. Woods, J.J. Xu, K. M. Yarborough, J.G. Hengstler, Recent advances in 2D and 3D in vitro systems using primary hepatocytes, alternative hepatocyte sources and non-parenchymal liver cells and their use in investigating mechanisms of hepatotoxicity, cell signaling and ADME, Arch. Toxicol. 87 (2013) 1315–1530.

[14] B. Kwak, Y. Lee, J. Lee, S. Lee, J. Lim, Mass fabrication of uniform sized 3D tumor spheroid using high-throughput microfluidic system, J. Control. Release 275 (2018) 201–207.

[15] S. Sant, P.A. Johnston, The production of 3D tumor spheroids for cancer drug discovery, Drug Discovery Today: Technologies 23 (2017) 27–36.

[16] M. Singh, D.A. Close, S. Mukundan, P.A. Johnston, S. Sant, Production of Uniform 3D Microtumors in Hydrogel Microwell Arrays for Measurement of Viability, Morphology, and Signaling Pathway Activation, Assay Drug Dev. Technol. 13 (2015) 570–583.

[17] M. Cheray, G. Begaud, E. Deluche, A. Nivet, S. Battu, F. Lalloue, M. Verdier, B. Bessette, Cancer Stem-Like Cells in Glioblastoma, 2017.

[18] E. Batlle, H. Clevers, Cancer stem cells revisited, Nat. Med. 23 (2017) 1124–1134.

[19] P.O. Guichet, S. Guelfi, C. Ripoll, M. Teigell, J.C. Sabourin, L. Bauchet, V. Rigau, B. Rothhut, J.P. Hugnot, Asymmetric Distribution of GFAP in Glioma Multipotent Cells, PLoS One 11 (2016).

[20] W.H. Matsui, Cancer stem cell signaling pathways, Medicine 95 (2016).

[21] C.Y. Zhang, Z.T. Yang, D.L. Dong, T.S. Jang, J.C. Knowles, H.W. Kim, G.Z. Jin, Y. H. Xuan, 3D culture technologies of cancer stem cells: promising ex vivo tumor models, J. Tissue Eng. 11 (2020).

[22] S. Dawood, L. Austin, M. Cristofanilli, Cancer Stem Cells: Implications for Cancer Therapy, Oncology-NY 28 (2014) 1101. -+.

[23] M. Luo, J.F. Li, Q. Yang, K. Zhang, Z.W. Wang, S. Zheng, J.J. Zhou, Stem cell quiescence and its clinical relevance, World J. Stem Cells 12 (2020).

[24] S.K. Singh, C. Hawkins, I.D. Clarke, J.A. Squire, J. Bayani, T. Hide, R. M. Henkelman, M.D. Cusimano, P.B. Dirks, Identification of human brain tumour initiating cells, Nature 432 (2004) 396–401.

[25] K.D. Caldwell, Z.Q. Cheng, P. Hradecky, J.C. Giddings, Separation of human and animal cells by steric field-flow fractionation, Cell Biophysics 6 (1984) 233–251.

[26] G. Bégaud-Grimaud, S. Battu, D.Y. Leger, P.J.P. Cardot, Mammalian Cell Sorting with Sedimentation Field Flow Fractionation, in: S.K.R. Williams, K.D. Caldwell (Eds.), Field-Flow Fractionation in Biopolymer Analysis, Springer-Verlag, Wien, 2012.

[27] A. Lacroix, E. Deluche, L.Y. Zhang, C. Dalmay, C. Melin, J. Leroy, M. Babay, C. M. Du Puch, S. Giraud, B. Bessette, G. Begaud, S. Saada, C. Lautrette, A. Pothier, S. Battu, F. Lalloue, A New Label-Free Approach to Glioblastoma Cancer Stem Cell Sorting and Detection, Anal. Chem. 91 (2019) 8948–8957.

[28] K.D. Caldwell, Steric field-flow fractionation and steric transition, in: M.E. Schimpf, K.D. Caldwell, J.C. Giddings (Eds.), Field-flow fractionation handbook, John Wiley & Sons, Inc., New York, 2000, pp. 79–94.

[29] S. Battu, W. Elyaman, J. Hugon, P.J.P. Cardot, Cortical cell elution by sedimentation field-flow fractionation, Biochim. Biophys. Acta 1528 (2001) 89–96.

[30] D.Y. Leger, S. Battu, B. Liagre, P.J.P. Cardot, J.L. Beneytout, Sedimentation field flow fractionation to study human erythroleukemia cell megakaryocytic differentiation after short period diosgenin induction, J. Chromatogr. A 1157 (2007) 309–320.

[31] P.-A. Faye, N. Vedrenne, M.A. De la Cruz-Morcillo, C.-C. Barrot, L. Richard, S. Bourthoumieu, F. Sturtz, B. Funalot, A.-S. Lia, S. Battu, New Method for Sorting Endothelial and Neural Progenitors from Human Induced Pluripotent Stem Cells by Sedimentation Field Flow Fractionation, Anal. Chem. 88 (2016) 6696–6702.

[32] C. Mélin, A. Perraud, H. Akil, M.O. Jauberteau, P. Cardot, M. Mathonnet, S. Battu, Cancer Stem Cell Sorting from Colorectal Cancer Cell Lines by Sedimentation Field Flow Fractionation, Anal. Chem. 84 (2012) 1549–1556.

[33] J. Bertrand, G. Begaud-Grimaud, B. Bessette, M. Verdier, S. Battu, M.O. Jauberteau, Cancer stem cells from human glioma cell line are resistant to Fas-induced apoptosis, Int. J. Oncol. 34 (2009) 717–727.

[34] T. Sayde, R. Manczak, S. Saada, G. Begaud, B. Bessette, G. Lespes, P.Le Coustumer, K. Gaudin, C. Dalmay, A. Pothier, F. Lalloue, S. Battu, Characterization of Glioblastoma Cancer Stem Cells Sorted by Sedimentation Field-Flow Fractionation Using an Ultrahigh-Frequency Range Dielectrophoresis Biosensor, Anal. Chem. 93 (2021) 12664–12671.

[35] E.A. Aisenbrey, W.L. Murphy, Synthetic alternatives to Matrigel, Nat. Rev. Mater. 5 (2020) 539–551.

[36] E.R. Draper, D.J. Adams, Low-Molecular-Weight Gels: The State of the Art, Chem 3 (2017) 390–410.

[37] O. El Hamoui, K. Gaudin, S. Battu, P. Barthelemy, G. Lespes, B. Alies, Self-Assembly of Nucleoside-Derived Low-Molecular-Weight Gelators: A Thermodynamics and Kinetics Study on Different Length Scales, Langmuir 37 (2021) 297–310.

[38] M.A. Ramin, L. Latxague, K.R. Sindhu, O. Chassande, P. Barthelemy, Low molecular weight hydrogels derived from urea based-bolaamphiphiles as new injectable biomaterials, Biomaterials 145 (2017) 72–80.

[39] O. El Hamoui, T. Sayde, I. Svahn, A. Gudin, E. Gontier, P. Le Coustumer, J. Verget, P. Barthelemy, K. Gaudin, S. Battu, G. Lespes, B. Alies, Nucleoside-Derived Low-Molecular-Weight Gelators as a Synthetic Microenvironment for 3D Cell Culture, ACS Biomater. Sci. Eng. 8 (2022) 3387–3398.

[40] G. Bégaud-Grimaud, S. Battu, B. Liagre, J.L. Beneytout, M.O. Jauberteau, P.J. P. Cardot, Development of a downscale sedimentation field flow fractionation device for biological event monitoring, J. Chromatogr. A 1216 (2009) 9125–9133.

[41] P.S. Williams, S. Lee, J.C. Giddings, Characterization of hydrodynamic lift forces by field-flow fractionation. Inertial and near-wall lift forces, Chem. Eng. Commun. 130 (1994) 143–166.

[42] M.E. Buczek, S.P. Reeder, T. Regad, Identification and Isolation of Cancer Stem Cells Using NANOG-EGFP Reporter System, in: G. Papaccio, V. Desiderio (Eds.), Cancer Stem Cells: Methods and Protocols, Humana Press Inc, Totowa, 2018, pp. 139–148.

[43] I.S. Mohiuddin, S.J. Wei, M.H. Kang, Role of OCT4 in cancer stem-like cells and chemotherapy resistance, Biochimica Et Biophysica Acta-Molecular Basis of Disease 1866 (2020).

[44] D. Zeineddine, A. Hammoud, M. Mortada, H. Boeuf, The Oct4 protein: more than a magic stemness marker, Am J Stem Cells 3 (2014) 74–82.

[45] F.Y. Zhu, W.Q. Qian, H.J. Zhang, Y. Liang, M.Q. Wu, Y.Y. Zhang, X.H. Zhang, Q. Gao, Y. Li, SOX2 Is a Marker for Stem-like Tumor Cells in Bladder Cancer, Stem Cell Rep 9 (2017) 429–437.

[46] X. Jin, X. Jin, H. Kim, Cancer stem cells and differentiation therapy, Tumour Biol 39 (2017).

[47] E. Vlashi, F. Pajonk, Cancer stem cells, cancer cell plasticity and radiation therapy, Semin. Cancer Biol. 31 (2015) 28–35.

[48] P. Sancho, D. Barneda, C. Heeschen, Hallmarks of cancer stem cell metabolism, Br. J. Cancer 114 (2016) 1305–1312.

[49] X. Liu, A.B. Hummon, Quantitative Determination of Irinotecan and the Metabolite SN-38 by Nanoflow Liquid Chromatography-Tandem Mass Spectrometry in Different Regions of Multicellular Tumor Spheroids, J. Am. Soc. Mass Spectrom. 26 (2015) 577–586.

[50] J.K. Lukowski, A.B. Hummon, Quantitative evaluation of liposomal doxorubicin and its metabolites in spheroids, Anal. Bioanal. Chem. 411 (2019) 7087–7094.

[51] K.M. McMahon, M. Volpato, H.Y. Chi, P. Musiwaro, K. Poterlowicz, Y. Peng, A. J. Scally, L.H. Patterson, R.M. Phillips, C.W. Sutton, Characterization of Changes in the Proteome in Different Regions of 3D Multicell Tumor Spheroids, J. Proteome Res. 11 (2012) 2863–2875.

[52] L. Persano, E. Rampazzo, G. Basso, G. Viola, Glioblastoma cancer stem cells: Role of the microenvironment and therapeutic targeting, Biochem. Pharmacol. 85 (2013) 612–622.